Inorganic Chemistry

Article

pubs.acs.org/IC

Tunable Luminescence and Application in Dye-Sensitized Solar Cells of Zn(II)/Hg(II) Complexes: Methyl Substitution-Induced Supramolecular Structures Based on (*E*)-*N*-(6-Methoxypyridin-2-ylmethylene)arylamine Derivatives

Yu-Wei Dong,[†] Rui-Qing Fan,*[,†] Ping Wang,[†] Li-Guo Wei,[†] Xin-Ming Wang,[†] Song Gao,[†] Hui-Jie Zhang,[†] Yu-Lin Yang,*[,†] and Yu-Lei Wang[‡]

[†]Department of Chemistry, Harbin Institute of Technology, Harbin 150001, People's Republic of China

[‡]National Key Laboratory of Science and Technology on Tunable Laser, Harbin Institute of Technology, Harbin 150080, People's Republic of China

Supporting Information

ABSTRACT: Using Schiff-base ligands (*E*)-*N*-(6-methoxypyridin-2-yl)(CH═NAr) (where Ar = C_6H_5, $\mathbf{L_1}$; 2-MeC_6H_4, $\mathbf{L_2}$; 2,4,6-$Me_3C_6H_2$, $\mathbf{L_3}$), six Zn(II)/Hg(II) complexes, namely, [Zn$\mathbf{L_1}Cl_2$] (**Zn1**), [Hg$\mathbf{L_1}Cl_2$] (**Hg1**), [Zn$\mathbf{L_2}Cl_2$] (**Zn2**), [Hg$\mathbf{L_2}Cl_2$] (**Hg2**), [Zn$\mathbf{L_3}Cl_2$] (**Zn3**), and [Hg$\mathbf{L_3}Cl_2$] (**Hg3**) have been synthesized under solvothermal conditions. The structures of six complexes have been established by X-ray single-crystal analysis and further physically characterized by EA, FT-IR, ^{1}H NMR, and ESI-MS. The crystal structures of these complexes indicate that noncovalent interactions, such as hydrogen bonds, C−H···Cl, and $\pi\cdots\pi$ stacking, play essential roles in constructing the resulting supramolecular structures (1D for **Hg3**; 2D for **Zn2**, **Hg2**; 3D for **Zn1**, **Hg1**, and **Zn3**). Upon irradiation with UV light, the emission of complexes **Zn1**−**Zn3** and **Hg1**−**Hg3** could be finely tuned from green (480−540 nm) in the solid state to blue (402−425 nm) in acetonitrile solution. It showed that the ligand and metal cation can influence the structures and luminescence properties of complexes such as emission intensities and maximum wavelengths. Since these ligands and complexes could compensate for the absorption of N719 in the low-wavelength region of the visible spectrum and reduce charge recombination of the injected electron, the ligands $\mathbf{L_1}$−$\mathbf{L_3}$ and complexes **Zn3**/**Hg3** were employed to prepare cosensitized dye-sensitized solar cells devices for investigating the influences of the electron-donating group and coordination on the DSSCs performance. Compared to DSSCs only being sensitized by N719, these prepared ligands and complexes chosen to cosensitize N719 in solar cell do enhanced its performance by 11−41%. In particular, a DSSC using $\mathbf{L_3}$ as cosensitizer displays better photovoltaic performance with a short circuit current density of 18.18 mA cm^{-2}, corresponding to a conversion efficiency of 7.25%. It is much higher than that for DSSCs only sensitized by N719 (5.14%).

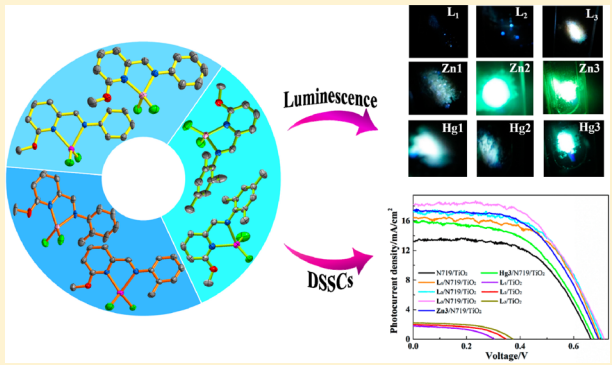

INTRODUCTION

Inorganic−organic optoelectronic materials are underlying candidates for the burgeoning technologies of luminescence and green-energy applications.[1−3] After the first reports of a dye-sensitized solar cells (DSSCs) device,[4−6] extensive attention has been paid to this area. However, a combination of intense luminescence and high efficiency of cosensitizing DSSCs in these materials is relatively uncommon. From the point of molecular design, it is important to design and synthesize a new complex with the excellent advantages of luminescence and DSSCs.[7] In particular, the complexes have been studied in the development and application of luminescent materials in recent years as they have a degree of structural predictability: metal-based binding sites and organic linkers in crystalline form.[8] The complexes which adopt the combination form of d^{10} metals and aromatic organic linkers display stable structure and intense luminescence. In addition, detailed studies on transition complexes have further demonstrated that organic ligands play vital roles in influencing the luminescent color and intensity. In the design of complexes, Schiff bases have been widely used as ligands due to their developed synthetic chemistry.[9] Meanwhile, in the design of DSSCs, the great challenge is the spectral mismatch.[10] To solve this problem and further improve the efficiency of the device, it is more meaningful to attempt the method of cosensitization to extending the light-harvesting spectrum.[11] Although some organic molecules and complexes have been developed as

Received: March 24, 2015
Published: July 24, 2015

DOI: 10.1021/acs.inorgchem.5b00661
Inorg. Chem. 2015, 54, 7742−7752

Scheme 1. Syntheses and Conversion of Three Ligands L_1–L_3 and Six Corresponding Zn(II)/Hg(II) Complexes

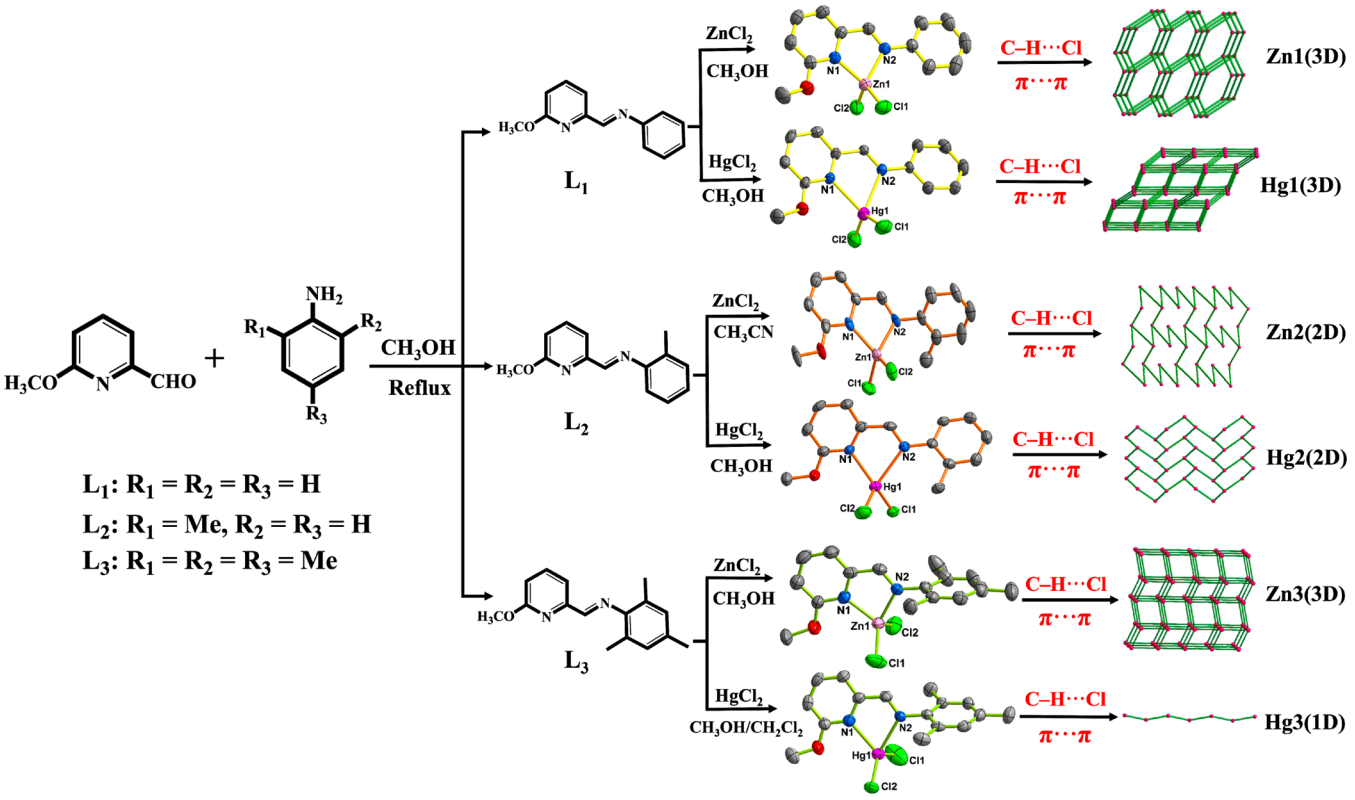

cosensitizers in DSSCs, design and synthesis of organic ligands and their metal complexes for application on DSSCs is still a great challenge.

To better explore efficient light-management strategies with the respect to tunable luminescence and high-efficiency cosensitization for DSSCs,[12] we have been devoted to the photophysics of transition metal complexes recently, such as those containing Zn(II) and Hg(II) complexes.[13,14] Herein, the synthesis of three new Schiff-base ligands (*E*)-*N*-(6-methoxypyridin-2-yl)(CH═NAr) (Ar = C_6H_5, L_1; 2-MeC_6H_4, L_2; 2,4,6-$Me_3C_6H_2$, L_3) and their Zn(II)/Hg(II) complexes with different supermolecular structures $[ZnL_1Cl_2]$ (**Zn1**), $[HgL_1Cl_2]$ (**Hg1**), $[ZnL_2Cl_2]$ (**Zn2**), $[HgL_2Cl_2]$ (**Hg2**), $[ZnL_3Cl_2]$ (**Zn3**), and $[HgL_3Cl_2]$ (**Hg3**) are presented (Scheme 1). Their tunable luminescence to different central metals and functional groups are studied. Importantly, the ligands L_1–L_3 and complexes **Zn3**/**Hg3** were employed to prepare cosensitized DSSCs devices, which could compensate for the absorption of N719 in the high-energy band region of the visible spectrum. Thus, the performance of DSSCs based on ligands L_1–L_3 and complexes **Zn3**/**Hg3** as cosensitizers is investigated in detail.

RESULTS AND DISCUSSION

Synthetic and Spectral Aspects. As shown in Scheme 1, three novel Schiff-base ligands (*E*)-*N*-(6-methoxypyridin-2-yl)(CH═NAr) (Ar = C_6H_5, L_1; 2-MeC_6H_4, L_2; 2,4,6-$Me_3C_6H_2$, L_3) have been synthesized by reactions of 6-methoxy-2-pyridinecarboxaldehyde with aniline derivates in a 1:1 molar ratio. Moreover, the yellow bulk crystals of L_3 were obtained by recrystallization from methanol. Using a self-assembled method, these ligands were reacted with Zn(II)/Hg(II) chloride at refluxing temperature to obtain a series of complexes, namely, **Zn1**–**Zn3** and **Hg1**–**Hg3**. X-ray quality single crystals of six Zn(II)/Hg(II) complexes were grown from slow evaporation of their solutions and readily obtained in good yield within the range of 54–73%. The details of the synthesis are given in the Experimental Section. The yellow solids **Zn1**–**Zn3** and **Hg1**–**Hg3** were found to be stable enough to store under ambient conditions for several months. The complexes show good solubility in chloroform, dimethyl sulfoxide, and acetonitrile solvents. The identities of L_1–L_3, **Zn1**–**Zn3**, and **Hg1**–**Hg3** are established by satisfactory EA, FT-IR, ESI-MS, and ^{1}H NMR spectra.

The FT–IR spectra of all six complexes (Figures S1–S3, Supporting Information) are similar to that of the corresponding ligand, and selected diagnostic bands are listed in the experimental section. The stretching vibrations of C═N (1620–1637 cm^{-1}) in the complexes are slightly red shifted compared with that of the ligands (1629–1646 cm^{-1}), which proved the coordination between the imine nitrogen atoms of L_1–L_3 and Zn(II)/Hg(II) atoms.[15] Meanwhile, they show ν_{Ar-H} and ν_{C-O} vibrations around 1460–1600 and 1226–1299 cm^{-1}, respectively. The characteristic ν_{M-N} of the complexes occurs at 435–478 cm^{-1}. The ^{1}H NMR spectra of L_1–L_3 (Figures S4–S6, Supporting Information) show that the resonances of the −C*H*═N− protons appear at 8.20–8.48 ppm. Further, these signals shift toward low field, which appear at 8.37–8.64 ppm for the corresponding **Zn1**–**Zn3** and **Hg1**–**Hg3**.[16] The resonance peaks at ca. 6.81–8.16 and 3.98–4.29 ppm are assigned to the protons on the pyridine/phenyl rings and −OCH_3 protons of pyridine rings, respectively. In complexes of L_2 and L_3, the difference between them only is the number of −CH_3 of the phenyl ring, for which the methyl protons appear at 2.38–2.43 and 2.13–2.30 ppm, respectively. Meanwhile, the compositions of the ligands and complexes

DOI: 10.1021/acs.inorgchem.5b00661
Inorg. Chem. 2015, 54, 7742–7752

Table 1. Crystal Structure Refinement Data of L_3, Zn1−Zn3, and Hg1−Hg3

	Zn1	Hg1	Zn2	Hg2	L_3	Zn3	Hg3
CCDC no.	1046956	1046957	1046958	1046959	1046960	1046961	1046962
formula	$C_{13}H_{12}Cl_2N_2OZn$	$C_{13}H_{12}Cl_2N_2OHg$	$C_{14}H_{14}Cl_2N_2OZn$	$C_{14}H_{14}Cl_2N_2OHg$	$C_{16}H_{18}N_2O$	$C_{16}H_{18}Cl_2N_2OZn$	$C_{16}H_{18}Cl_2N_2OHg$
M_r	348.54	483.74	362.56	497.76	254.32	390.61	525.81
cryst syst	triclinic	monoclinic	triclinic	monoclinic	monoclinic	triclinic	monoclinic
space group	$P\bar{1}$	$C2/c$	$P\bar{1}$	$P2_1/c$	$P2_1/c$	$P\bar{1}$	Pc
a [Å]	7.996(16)	20.365(9)	7.981(16)	12.827(2)	14.850(8)	7.896(16)	15.246(3)
b [Å]	9.378(19)	8.324(3)	16.462(3)	7.754(15)	17.003(6)	8.027(16)	7.587(15)
c [Å]	11.060(2)	17.230(5)	19.508(4)	18.210(2)	12.566(7)	15.009(3)	16.816(3)
α [deg]	85.71(3)	90	68.04(3)	90	90	82.46(3)	90
β [deg]	77.61(3)	93.36(3)	83.45(3)	121.45(9)	112.04(6)	82.35(3)	111.32(3)
γ [deg]	65.13(3)	90	77.33(3)	90	90	72.42(3)	90
vol. [Å^3]	734.9(2)	2916.2(19)	2317.7(8)	1545.2(4)	2941.2(3)	894.6(3)	1812.2(6)
Z	2	8	6	4	8	2	2
D_c [g·cm^{-3}]	1.575	2.204	1.559	2.140	1.149	1.450	0.964
μ [mm^{-1}]	2.026	10.914	1.931	10.302	0.073	1.673	4.395
F (000)	352	1808	1104	936	1088	400	500
Θ range [deg]	3.02−27.48	3.51−27.56	3.02−25.00	1.86−26.94	3.46−27.56	3.12−25.00	3.04−24.99
h range	$-10 \le h \le 9$	$-26 \le h \le 25$	$-8 \le h \le 9$	$-15 \le h \le 16$	$-10 \le h \le 19$	$-9 \le h \le 8$	$-18 \le h \le 18$
k range	$-12 \le k \le 12$	$-9 \le k \le 10$	$-19 \le k \le 19$	$-9 \le k \le 9$	$-22 \le k \le 17$	$-9 \le k \le 9$	$-9 \le k \le 9$
l range	$-14 \le l \le 14$	$-8 \le l \le 22$	$-22 \le l \le 23$	$-20 \le l \le 21$	$-16 \le l \le 11$	$-16 \le l \le 17$	$-19 \le l \le 19$
data/restraints/ params	3267/0/172	3331/0/173	8075/19/517	3094/0/182	6726/0/352	3056/0/199	3113/2/199
GOF	1.038	0.992	1.109	0.992	0.979	1.007	1.005
R_1, wR_2 [$I > 2\sigma(I)$]	0.0418, 0.1020	0.0438, 0.0665	0.0724, 0.1873	0.0377, 0.0878	0.0673, 0.1708	0.0535, 0.1456	0.0284, 0.0608
R_1, wR_2 [all data]	0.0596, 0.1208	0.0712, 0.0772	0.0845, 0.1925	0.0485, 0.0936	0.1412, 0.2199	0.0866, 0.1743	0.0301, 0.0619
$\Delta\rho_{max}$, $\Delta\rho_{min}$ [e·Å^{-3}]	0.466, −0.377	0.857, −1.066	2.091, −1.982	2.676, −1.622	0.382, −0.151	0.418, −0.385	0.648, −0.240

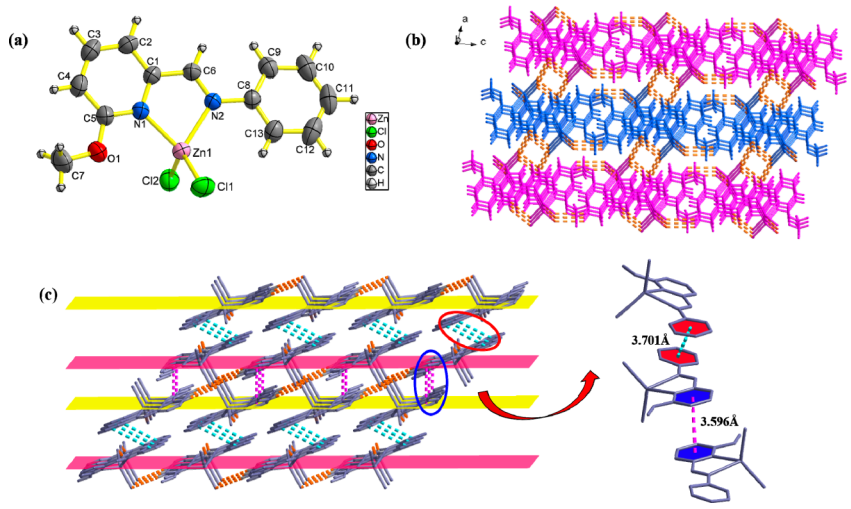

Figure 1. (a) Crystal structure of **Zn1**. Thermal ellipsoid is drawn at 50% probability. (b) The 3D network structure in **Zn1**. (c) The 3D network structure in **Hg1**. Dotted lines represent the C−H···Cl and $\pi\cdots\pi$ interactions.

have also been supported by ESI-MS studies (Figure S7, Supporting Information). We performed powder X-ray diffraction patterns on ligand $\mathbf{L_3}$ and six Zn(II)/Hg(II) complexes to check the purity of the bulk products. From Figures S8−S14, Supporting Information, we can see that all major peak positions of the measured patterns are in good agreement with those simulated. Furthermore, the differences in intensity may be due to the preferred orientation of the crystal products.[17]

Structural Description of $[ZnL_1Cl_2]$ (Zn1) and $[HgL_1Cl_2]$ (Hg1). Considering that complexes **Zn1** and **Hg1** are isostructural, we choose **Zn1** to represent the detailed structure. Complex **Zn1** belongs to the triclinic $P\bar{1}$ space group, while complex **Hg1** belongs to monoclinic $C2/c$ space group. The detailed data of crystal structure refinement for **Zn1** and **Hg1** are listed in Table 1. The crystal structure of **Zn1** is described in Figure 1a together with the atomic numbering scheme. The Zn(II) center adopts a distorted tetrahedral geometry (Figure S15a, Supporting Information) coordinated by two nitrogen atoms of *N*-((6-methoxypyridin-2-yl)methylene)aniline ($\mathbf{L_1}$) and two terminal chlorine ions. In particular, the Zn(II) cation coordinates with nitrogen atoms from ligand $\mathbf{L_1}$ to form a five-membered ring, which further extends system conjugatation. Complexes **Zn1** and **Hg1** have dihedral angles of 9.879(1)° and 15.113(2)°, respectively, between the pyridyl ring and the phenyl ring (Table S1, Supporting Information), which indicates that the ligand $\mathbf{L_1}$ displays better coplanarity in **Zn1** than **Hg1**. The distances of Zn1−N1 and Zn1−N2 are

DOI: 10.1021/acs.inorgchem.5b00661
Inorg. Chem. 2015, 54, 7742−7752

2.058(3) and 2.099(3) Å, in agreement with the values of a similar zinc complex.[18] The distance of Zn1−Cl2 (2.216(1) Å) is slightly longer than that of Zn1−Cl1 (2.202(1) Å). The detailed bond distances and angles are listed in Table S2, Supporting Information. In complex **Zn1**, the independent units are linked through C6−H6A···Cl1 hydrogen bonds[19] to generate a one-dimensional double chains (Figure S15b, Supporting Information). There are two-dimensional layers in the *ac* plane interconnected by C3−H3A···Cl2 hydrogen bonds (Figure S15c, Supporting Information). As shown in Figure 1b, the two-dimensional layers are further linked by C10−H10A···Cl2 hydrogen bonds, resulting in construction of a three-dimensional supramolecular network. Three additional intermolecular $\pi\cdots\pi$ interactions with separations of about 3.638, 3.753, and 3.795 Å (Figure S15d, Supporting Information) also provide further stabilization. The detailed data of the noncovalent bond interactions (C−H···Cl and $\pi\cdots\pi$) for all complexes are listed in Tables S3 and S4, Supporting Information, respectively. The final supramolecular architecture can be simplified into a three-dimensional topology structure (Figure S16, Supporting Information) under the circumstance of the mononuclear unit viewed as the node and the C−H···Cl hydrogen bonds as linkers.[20]

In addition, the structure of **Hg1** is shown in Figure S17a, Supporting Information. Although complexes **Zn1** and **Hg1** are isostructural, due to the coordination of the different center metals to the ligand $\mathbf{L_1}$, their supramolecular structures are obviously different. In **Hg1**, the $\pi\cdots\pi$ stacking interactions play key roles to form the three-dimensional structures. As shown in Figure 1c, a 3D network can be constructed by interlayer $\pi_{pyridyl}\cdots\pi_{pyridyl}$ (3.596 Å) and $\pi_{phenyl}\cdots\pi_{phenyl}$ (3.701 Å) stacking interactions. The overall topology of **Hg1** is illustrated in Figure S17b, Supporting Information.

Structural Description of $[ZnL_2Cl_2]$ (Zn2) and $[HgL_2Cl_2]$ (Hg2). Crystal refinement data of complex **Zn2** implied that it belongs to a triclinic system, $P\bar{1}$ space group. The asymmetric unit consists of three crystallographically and conformationally independent molecules as shown in Figure 2a. In **Zn2** all three

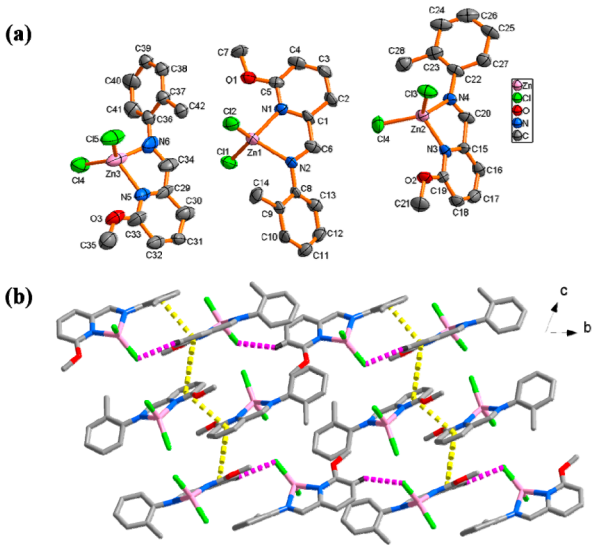

Figure 2. (a) Crystal structure of **Zn2** (hydrogen atoms are omitted for clarity). Thermal ellipsoid is drawn at 50% probability. (b) The 2D layer structure of **Zn2**. Dotted lines represent the C−H···Cl and $\pi\cdots\pi$ interactions.

zinc atoms are bonded to six nitrogen atoms with similar distances varying from 2.031(7) to 2.164(7) Å (Table S5, Supporting Information). The bond angles around the Zn(II) ion are in the range of 79.2(3)−121.8(2)°. The pyridyl ring and phenyl ring display different torsion angles: 48.341(2)°, 59.240(2)°, and 85.294(2)°. Compared to **Zn2**, the X-ray structure of **Hg2** consists of one Hg(II) cation, two coordinated chlorine ions, and one $\mathbf{L_2}$ ligand, as displayed in Figure S18, Supporting Information. The bond distances around Hg1 are 2.270(5) (Hg1−N1), 2.504(5) (Hg1−N2), 2.428(2) (Hg1−Cl1), and 2.382(2) Å (Hg1−Cl2). Single-crystal analysis shows that complexes **Zn2** and **Hg2** are both two-dimensional layer structures (Figures 2b and S19a, respectively, Supporting Information) constructed by the C−H···Cl (Table S3, Supporting Information) and $\pi\cdots\pi$ interactions (Table S4, Supporting Information). Similarly, the overall topology of **Zn2** and **Hg2** can be defined as a two-dimensional layer, as illustrated in Figures S20 and S19b, Supporting Information, respectively.

Structural Description of L_3 and $[ZnL_3Cl_2]$ (Zn3) and $[HgL_3Cl_2]$ (Hg3). Reactions of $\mathbf{L_3}$ with MCl_2 gave two isostructural complexes **Zn3** and **Hg3**. Therefore, the crystal structure of **Zn3** is only described in detail. The detailed data of crystal structure refinement for $\mathbf{L_3}$, **Zn3**, and **Hg3** are listed in Table 1. After recrystallization from methanol, the yellow block crystals of ligand $\mathbf{L_3}$ were obtained. The crystal structure of ligand $\mathbf{L_3}$ is shown in Figure 3a. The distance between N2 and C6 is 1.259(3) Å, indicating C=N double-bond character.[21] The dihedral angle (64.606°) between pyridine ring and phenyl ring is deviated from a perpendicular structure due to the steric hindrance effect. Moreover, the value of the N1−C1−C6−N2 torsion angle is 174.1(2)°. As shown in Figure 3b and 3c, the coordination number of M(II) is four with two nitrogen atoms from ligand $\mathbf{L_3}$ and two terminal chlorine atoms. Between pyridine ring and phenyl ring, the dihedral angles are 89.217(1)° (**Zn3**) and 69.030(1)° (**Hg3**), which are approximately perpendicular compared with those of complexes **Zn1** and **Hg1**. The order of the dihedral angle is **Zn3**, **Hg3** > **Zn2**, **Hg2** > **Zn1**, **Hg1**, and this is because of the biggest steric hindrance of 2,4,6-$(CH_3)_3$ substitution. In complexes **Zn3** and **Hg3**, the average Zn−N linkages (2.085 Å) are smaller than the average Hg−N linkages (2.395 Å), which is consistent with ionic radii. In addition, the N1−C1−C6−N2 torsion angles are −0.8(8)° (**Zn3**) and 0.3(9)° (**Hg3**), which are largely twisted compared to that in the free ligand $\mathbf{L_3}$ (174.1(2)°), as shown in Scheme 2. It can be easily explained that through the coordination interaction the structure becomes more stable. Although complexes **Zn3** and **Hg3** are isostructural, their supramolecular structures are obviously different because of the different ionic radii of the center metals (Zn(II) and Hg(II)). The mononuclear molecules of **Zn3** and **Hg3** are assembled into a 3D network (Figure S21a,b, Supporting Information) and 1D chain (Figure S22a,b, Supporting Information), respectively, by the intermolecular C−H···Cl and $\pi\cdots\pi$ interactions.

Luminescent Properties. It is well known that transition metal complexes play an increasingly important role in influencing the intensity and emission wavelength of ligands via metal coordination.[22] To better understand the luminescent mechanism in the solid state, the emission spectra (Figure 4) of $\mathbf{L_1}$−$\mathbf{L_3}$, **Zn1**−**Zn3**, and **Hg1**−**Hg3** have been carried out. Compared with the emission spectra of the ligands ($\mathbf{L_1}$, $\mathbf{L_2}$, and $\mathbf{L_3}$: 476, 497, and 513 nm), the emissions of **Zn1**−**Zn3** and

DOI: 10.1021/acs.inorgchem.5b00661
Inorg. Chem. 2015, 54, 7742−7752

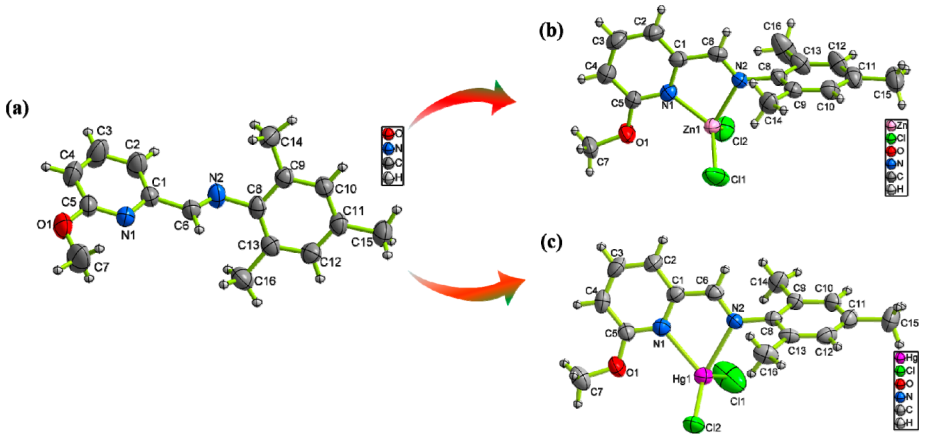

Figure 3. Crystal structure of (a) ligand L_3, (b) complex **Zn3**, and (c) complex **Hg3**. Thermal ellipsoid is drawn at 50% probability.

Scheme 2. Overlay Diagram of the L_3 Unit in Complexes Zn3 and Hg3

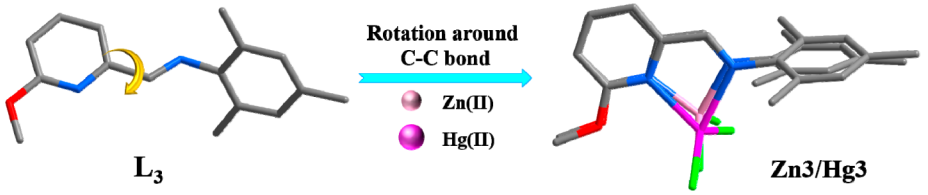

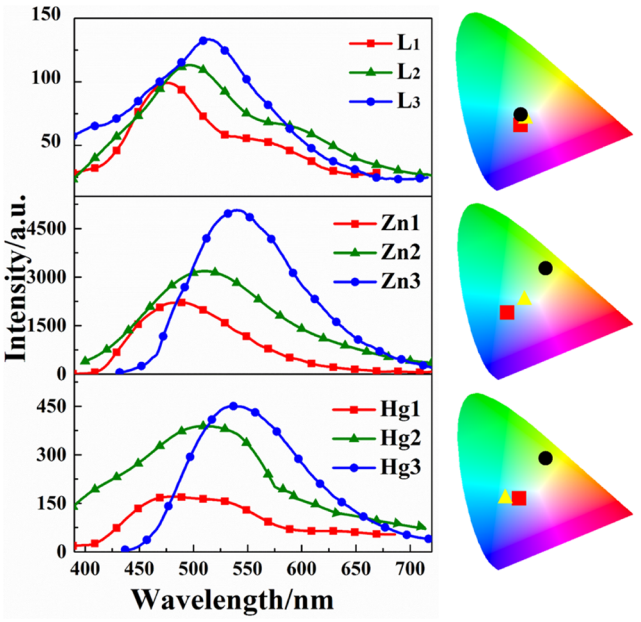

Figure 4. Emission spectra of L_1–L_3, **Zn1**–**Zn3**, and **Hg1**–**Hg3** in the solid state upon excitation with 365 nm, and CIE coordinates (■ = L_1, **Zn1**, and **Hg1**; ▲ = L_2, **Zn2**, and **Hg2**; ● = L_3, **Zn3**, and **Hg3**).

Hg1–**Hg3** are green luminescence (Figure 5a) with maxima at 488, 510, 540, 480, 506, and 537 nm. The luminescent mechanism of these complexes could be attributed to the ligand-centered π^*–π transition.[23] This result can be easily explained as three factors: (i) $ZnCl_2$/$HgCl_2$ themselves are nonluminance; (ii) Zn(II)/Hg(II) ions could not be oxidized or reduced due to their d^{10} configuration, and it is rarely in the nature of metal–to–ligand charge transfer (MLCT) and ligand–to–metal charge transfer (LMCT); (iii) the complexes **Zn1**–**Zn3** and **Hg1**–**Hg3** have similar emission energies to the corresponding ligand.[24] Notably, the emission intensity trend of this band for the complexes **Zn1**–**Zn3**/**Hg1**–**Hg3** series is in the sequence of **Zn1** < **Zn2** < **Zn3**, **Hg1** < **Hg2** < **Hg3** (similar to ligands L_1 < L_2 < L_3). It is fascinating that the number of methyls is in line with the emission intensity trend, namely, the methyl as an electron-donating group can induce the emission of the complex to stronger intensity in the solid state. Meanwhile, compared with the emission spectra of the ligands, the complexes show a red-shifted emission with intensities enhanced dramatically. This may be ascribed to the coordination of the free ligands L_1–L_3 to Zn(II)/Hg(II) ions, which results in enhancing the rigidity of organic molecules and decreasing the energy loss through vibration motions.[25] In particular, we find that **Zn3** possesses the strongest luminescence intensity among these six complexes (Figure 5b). This is interpreted as being due to the fact that there exists large conformational rigidity and electron-donating ability in **Zn3** with a 3D supramolecular architecture.

The maximum emission wavelengths of all complexes are in the range of 402–425 nm in acetonitrile solution and produce blue emission (the coordinates of CIE are in the blue region) (Figure 6). At 298 K, for six solid-state complexes, the maximum emission peaks are red shifted about 100 nm compare with those measured those in CH_3CN, which could be in the nature of the noncovalent forces in the solid state. The large red shift could be beneficial for reducing the energy gap of HOMO–LUMO and have an effect on the π^*–π transitions.[26] From the data of quantum yields (Table 2), we can see that the coordination between the metal M(II) center and the ligand notably enhances the quantum yields.[27] In particular, the quantum yield of **Zn3** (Φ_F = 0.206) is 4.57-fold to L_3 (Φ_F = 0.045). The quantum yields of **Hg1**–**Hg3** (Φ_F = 0.035–0.051) are much lower than those of **Zn1**–**Zn3** (Φ_F = 0.082–0.206), which are caused by the "heavy atom effect".[28] Due to the special sensitivity to Hg(II) ions with the luminescence intensity, it inspires us to further explore the valuable application as a luminescent sensor for Hg^{2+}.[29]

DOI: 10.1021/acs.inorgchem.5b00661
Inorg. Chem. 2015, 54, 7742–7752

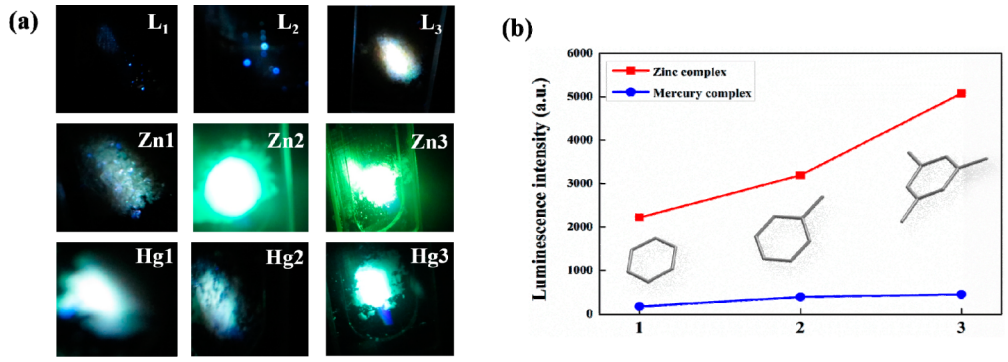

Figure 5. (a) Photographs of L_1−L_3, **Zn1**−**Zn3**, and **Hg1**−**Hg3** upon excitation with 365 nm. (b) Plot of the luminescence intensity of six Zn(II)/Hg(II) complexes (inset graph refers to the substituent group change in aniline).

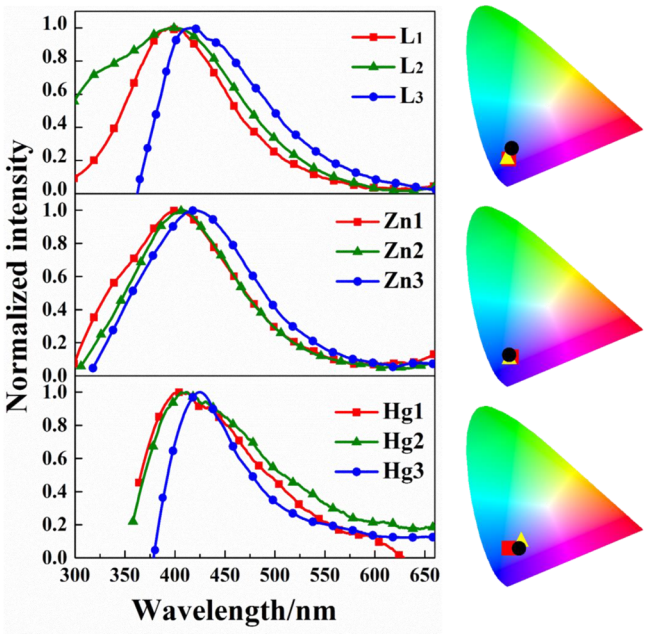

Figure 6. Emission spectra of L_1−L_3, **Zn1**−**Zn3**, and **Hg1**−**Hg3** in acetonitrile solution, and CIE coordinates (■ = L_1, **Zn1**, and **Hg1**; ▲ = L_2, **Zn2**, and **Hg2**; ● = L_3, **Zn3**, and **Hg3**).

In addition, the luminescence decay profiles of ligands and complexes were investigated. As indicated in Table S6, Supporting Information, the lifetimes of the complexes (τ = 7.63−12.62 μs for **Zn1**−**Zn3**; τ = 5.16−8.83 μs for **Hg1**−**Hg3**) are longer than those of the corresponding ligands L_1−L_3 (τ = 3.90−5.82 μs), which proves that coordination between ligand and mental centers is beneficial for stabilizing the structure.[30] The solid-state luminescence lifetimes are much longer than those in CH_3CN, which might be explained by the fact that there is a less polar nature in the solid-state environment.[31] Meanwhile, the lifetimes of **Hg1**−**Hg3** (5.16−7.99 μs in acetonitrile solution; 7.10−8.83 μs in the solid state) are shorter than those of **Zn1**−**Zn3** (7.63−9.64 μs in acetonitrile solution; 10.78−12.62 μs in the solid state) by virtue of the heavy-atom effect of Hg(II).[32]

Application in Dye-Sensitized Solar Cells. *Electrochemical Properties.* We investigated the UV−vis absorption spectra of ligands L_1−L_3 along with the Zn(II)/Hg(II) complexes in ethanol (Figure S23, Supporting Information). From the UV−vis absorption spectra, it is easy to find that L_3, **Zn3**, and **Hg3** exhibit two energy absorption bands in the range of 318−322 and 350−355 nm. Compared with the absorption spectra of N719 (Figure S24, Supporting Information), apparently L_3, **Zn3**, and **Hg3** could better compensate for the absorption of N719 in the low-wavelength region of the visible spectrum.[33] Therefore, we first chose L_3, **Zn3**, and **Hg3** as cosensitizers to apply in the DSSCs device. From the UV−vis absorption data (Table 3) we can see that the free ligands L_1 and L_2 exhibit intense absorption bands at 341 (ε = 22 581 dm^3 $mol^{-1}cm^{-1}$) and 353 nm (23 847 dm^3 $mol^{-1}cm^{-1}$), respectively. The higher molar extinction coefficient indicates that they possess a better light-harvesting ability in this low-wavelength region compared with N719.[34] Meanwhile, the ligands have bare nitrogen atoms of pyridine, which could adsorb at the TiO_2 surface. Therefore, the ligands L_1 and L_2 also were used as cosensitizers to apply in the DSSCs device.

The HOMO and LUMO energy levels are crucial in selecting sensitizers for DSSCs, which were determined by cyclic voltammetry (CV) in a 0.1 M $TBAPF_6$/ethanol solution. The CV curves of the ligands L_1−L_3 and complexes **Zn3** and **Hg3** are shown in Figure S25, Supporting Information, and detailed data are compiled in Table 3. As estimated from the onset oxidation potentials in the cyclic voltammograms, these cosensitizers have low-lying highest occupied molecular orbital

Table 2. Luminescent Data for Schiff-Base Ligands L_1−L_3 and the Corresponding Zn(II)/Hg(II) Complexes

	λ_{em} (nm)	fwhm (nm)	τ (μs)	Φ_{PL}[a]	CIE (x, y)	medium (298 K)
L_1	395	114.43	4.26	0.018	0.18, 0.13	CH_3CN
	476	118.93	5.19		0.27, 0.31	solid
Zn1	402	127.79	7.63	0.082	0.19, 0.14	CH_3CN
	488	104.59	10.78		0.21, 0.32	solid
Hg1	405	174.33	5.16	0.035	0.18, 0.18	CH_3CN
	480	106.21	7.10		0.26, 0.34	solid
L_2	400	178.52	3.90	0.037	0.17, 0.14	CH_3CN
	497	153.53	5.61		0.29, 0.35	solid
Zn2	409	116.42	8.35	0.122	0.18, 0.14	CH_3CN
	510	132.41	11.79		0.28, 0.39	solid
Hg2	412	129.20	5.50	0.041	0.23, 0.22	CH_3CN
	506	164.21	7.50		0.20, 0.35	solid
L_3	415	122.30	5.11	0.045	0.19, 0.18	CH_3CN
	513	151.85	5.82		0.27, 0.36	solid
Zn3	421	123.65	9.64	0.206	0.18, 0.15	CH_3CN
	540	113.71	12.62		0.37, 0.53	solid
Hg3	425	75.59	7.99	0.051	0.22, 0.18	CH_3CN
	537	112.39	8.83		0.37, 0.53	solid

[a]Measured in CH_3CN solutions (~1.0 × 10^{-5} M).

DOI: 10.1021/acs.inorgchem.5b00661
Inorg. Chem. 2015, 54, 7742−7752

Table 3. Spectral and Electrochemical Properties for Cosensitizers L_1−L_3, Zn3, and Hg3

cosensitizers	λ_{abs}(nm)[a]	ε (dm^3 $mol^{-1}cm^{-1}$)[a]	E_{ox} (V vs. SCE)[b]	E_{0-0} (eV)[c]	E_{HOMO} (eV)[d]	E_{LUMO} (eV)[d]
L_1	341	22 581	0.79	2.87	−5.19	−2.32
L_2	353	23 847	0.71	2.96	−5.11	−2.15
L_3	362	25 424	0.65	2.97	−5.05	−2.08
Zn3	361	21 928	0.70	2.93	−5.10	−2.17
Hg3	356	20 423	0.77	2.83	−5.17	−2.34

[a]Solvent: EtOH (3×10^{-4} M). [b]Values determined by cyclic voltammetry. [c]Estimated from the intersection wavelengths of the normalized absorption and emission spectra. [d]The HOMO and LUMO can be calculated to the following equations: $-e(E^{ox}_{onset}V + 4.4\ V)$; LUMO (eV) = $E_{HOHO} + E_{0-0}$.

(HOMO) levels from −5.19 to −5.05 eV. As shown in Scheme 3, all HOMOs are lower than the redox potential of I^-/I_3^-

Scheme 3. Orbital Energy Levels of Cosensitizers (L_1−L_3, Zn3 and Hg3), TiO_2, and Electrolyte I^-/I_3^-

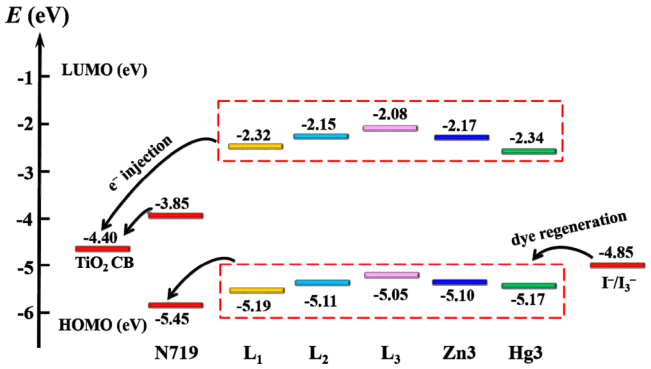

(−4.85 eV vs vacuum), indicating the favorable regeneration.[35,36] As calculated from the intersection of the normalized absorption and luminescence spectra, the zero−zero excitation energies (E_{0-0}) for L_1, L_2, L_3, **Zn3**, and **Hg3** are 2.87, 2.96, 2.97, 2.93, and 2.83 eV, respectively. The lowest unoccupied molecular orbital (LUMO) energy levels of L_1, L_2, L_3, **Zn3**, and **Hg3** calculated from $E_{HOMO} + E_{0-0}$ are −2.32, −2.15, −2.08, −2.17, and −2.34 eV, respectively.[37] All calculated LUMOs are higher than the conduction band of TiO_2 (−4.40 eV vs vacuum), indicating efficient electron injection. Thus, the thermodynamic force for electron injection and regeneration of the photo-oxidized dyes is sufficient.

Photovoltaic Properties of DSSCs. The ligands L_1−L_3 and complexes **Zn3** and **Hg3** were assembled into cosensitized DSSCs devices to study the influence of the electron-donating group and coordination on the DSSCs performance, and their respective photovoltaic performance was tested under irradiance of 100 mW cm^{-2} AM 1.5G sunlight. For comparison purpose, devices sensitized by the free ligands L_1−L_3 were also assembled under the same experimental conditions. The data of J_{sc}, V_{oc}, and *FF* for these devices are shown in Figure 7 and compiled in Table 4. The results indicate that the individually N719-sensitized device achieves a η value of 5.14% (with J_{sc} = 13.26 mA/cm^2, V_{oc} = 0.66 V, and *FF* = 0.58), while the devices individually sensitized by L_1, L_2, and L_3 were found to show a low η value of 0.26% (with J_{sc} = 1.77 mA/cm^2, V_{oc} = 0.30 V, and *FF* = 0.49), 0.35% (with J_{sc} = 1.97 mA/cm^2, V_{oc} = 0.34 V, and *FF* = 0.52), and 0.44% (with J_{sc} = 2.22 mA/cm^2, V_{oc} = 0.37 V, and *FF* = 0.53).

However, upon cosensitization, the J_{sc} and V_{oc} of cells are higher than those of the individually N719-sensitized device. The devices based on L_1/N719, L_2/N719, L_3/N719, **Zn3**/N719, and **Hg3**/N719 yield J_{sc} of 16.48, 17.21, 18.18, 17.36, and 15.95 mA/cm^2, V_{oc} of 0.70, 0.71, 0.71, 0.69, and 0.67 V, and *FF* of 0.59, 0.57, 0.56, 0.55, and 0.53, respectively. According to the results (Table 4), it was found that the η values of these devices L_1/N719, L_2/N719, L_3/N719, **Zn3**/N719, and **Hg3**/N719 are 6.73%, 6.96%, 7.25%, 6.62%, and 5.70%, respectively, that is, cells individually sensitized by N719 (5.14%) show relatively lower efficiency. On the basis of the results of the above data, there is a dramatic influence of the substituent group and coordination on the DSSCs performance, and the η values increase in the order L_1/N719 < L_2/N719 < L_3/N719 and **Hg3**/N719 < **Zn3**/N719 < L_3/N719.

In common with the luminescence properties mentioned above, the number of electron-donating group methyls is the key factor for influencing the η values of DSSCs, which determines related electrochemical properties. The enhancement of the L_3/N719 and L_2/N719 cosensitized DSSC performance may be due to the influence of the electron-

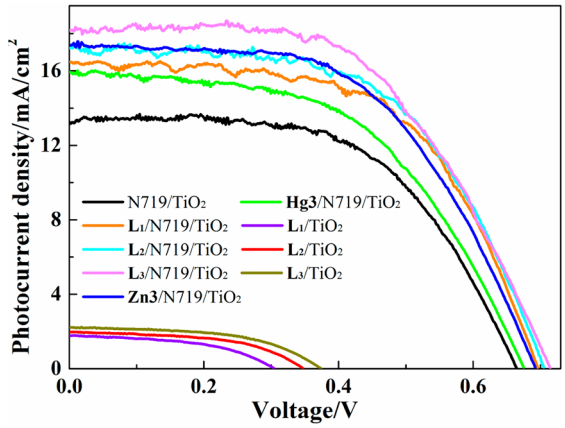

Figure 7. *J*−*V* curves of individually N719, L_1, L_2, and L_3 sensitized cells and cosensitized photoelectrodes cells under irradiance of 100 mW cm^{-2} AM 1.5G sunlight.

Table 4. Data of Photovoltaic Parameters of DSSCs with Different Photoelectrodes

photoelectrode	J_{sc} (mA/cm^2)	V_{oc} (V)	*FF*	η (%)
N719/TiO_2	13.26	0.66	0.58	5.14
L_1/TiO_2	1.77	0.30	0.49	0.26
L_2/TiO_2	1.97	0.34	0.52	0.35
L_3/TiO_2	2.22	0.37	0.53	0.44
L_1/N719/TiO_2	16.48	0.70	0.59	6.73
L_2/N719/TiO_2	17.21	0.71	0.57	6.96
L_3/N719/TiO_2	18.18	0.71	0.56	7.25
Zn3/N719/TiO_2	17.36	0.69	0.55	6.62
Hg3/N719/TiO_2	15.95	0.67	0.53	5.70

DOI: 10.1021/acs.inorgchem.5b00661
Inorg. Chem. 2015, 54, 7742−7752

donating group in the ligands (three methyls in $\mathbf{L_3}$, one methyl in $\mathbf{L_2}$, no methyl in $\mathbf{L_1}$). Notably, a DSSC using $\mathbf{L_3}$ as cosensitizer exhibits the highest efficiency (η) of 7.25%, which is 41% higher than that of the device individually sensitized by N719. The superior efficiency of the $\mathbf{L_3}$/N719 device can be ascribed to the higher light absorption ability in the visible range of the light spectrum. One probable explanation is that introduction of an electron-donating ($-CH_3$) group into the structure of the cosensitizers leads to the expansion and breadth of the absorption band, which is beneficial to improve the efficiency of devices,[38,39] that is, introduction of the methyl group brings about impressive changes (including the longer wavelength and bigger molar extinction coefficient) in the absorption spectra, which can further result in the performance of DSSCs. The aim of using complexes **Zn3**/**Hg3** as cosensitizers is to study the effect of coordination on the DSSCs performance. Although the conversion efficiency (η) of **Zn3**/N719 and **Hg3**/N719 is lower than that of $\mathbf{L_3}$/N719, it is still higher than that individually sensitized by N719. This may be due to the coordination of the metal and nitrogen that weakens the adsorption on the TiO_2 surface. Therefore, as a new type of cosensitizers, there are still many challenges to obtaining outstanding high conversion efficiency, especially the absorption spectra of the complexes lying at 300−450 nm.

The enhanced J_{sc} values will be discussed in conjunction with the incident photon-to-current electron conversion efficiency (IPCE) spectra in Figure 8, which are related by the equation $J_{sc} = \int e\phi_{ph.AM1.5G}(\lambda)d\lambda$.[40] The cell individually sensitized by N719 has a 300−750 nm broad IPCE spectrum, but in the wavelength range of 300−450 nm the intensity decreases. When the ligands $\mathbf{L_1}$−$\mathbf{L_3}$ and complexes **Zn3**/**Hg3** are used as cosensitizer, this decrease is efficiently inhibited as well as the IPCE spectra are enhanced in the visible region. These results can be attributed to the cosensitizers being absorbed on the TiO_2 surface effectively, which is beneficial for electron injection into the CB of the TiO_2. In other words, the cosensitization of N719 with the ligands $\mathbf{L_1}$−$\mathbf{L_3}$ and complexes **Zn3**/**Hg3** has a significant synergistic impact on light harvesting, electron collection, and electron injection on TiO_2. Taking the IPCE spectra as well as the absorption spectra into consideration, the better J_{sc} value of the cell with cosensitization is basically attributed to better light harvesting in the visible region, compensating for the absorption of N719.

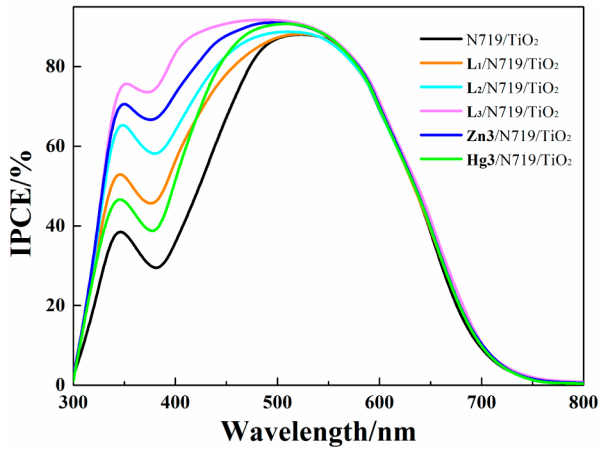

Figure 8. IPCE spectra for fabricated DSSCs with individually N719 sensitized and cosensitized with $\mathbf{L_1}$/N719, $\mathbf{L_2}$/N719, $\mathbf{L_3}$/N719, **Zn3**/N719, and **Hg3**/N719.

Electrochemical impedance spectroscopy (EIS) was carried out to elucidate the interfacial charge transfer process.[41] The EIS plots (Figure 9a) displayed two semicircles located in the high- and medium-frequency regions, a small semicircle can be assigned to charge transfer at Pt counter electrolyte, while the large semicircle can be attributed to the TiO_2/dye/electrolyte interface.[42] With the same counter electrode and electrolyte, small circles of devices were almost identical. However, the large semicircle demonstrates the resistance of the charge transfer from the TiO_2 to the electrolyte (R_{rec}). Figure 9a shows that the radius of the large semicircle increased after being cosensitized with the ligands $\mathbf{L_1}$−$\mathbf{L_3}$ and complexes **Zn3**/**Hg3**, implying more effective suppression of the back reaction generated from the injected electrons with I_3^- from electrolyte, yielding improvements of the photovoltage and substantially enhanced device efficiency. Under light illumination, as shown in Figure 9b, the radius of large- to medium-frequency semicircles decreases after cosensitization, and the order is $\mathbf{L_3}$/N719 < **Zn3**/N719 < $\mathbf{L_2}$/N719 < $\mathbf{L_1}$/N719 < **Hg3**/N719 < N719, which is in accord with the J_{sc}. Meanwhile, cosensitization not only decreases the electron transfer impedance but also increases the charge transfer rate of the interface. A higher charge transfer rate and lower charge recombination rate are beneficial for better DSSCs performance.

The devices were studied by the J−V curves in the dark to investigate the extent of back electron transfer.[43] Figure 10 shows the dark J−V characteristics of cells, which shows that cosensitized DSSCs in the dark display lower photocurrent compared with that of individual N719-sensitized DSSCs. According to the result of the enhanced onset potential and the

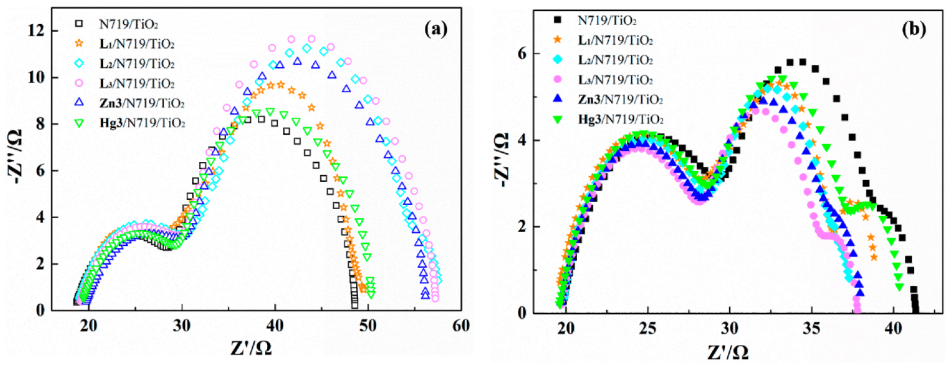

Figure 9. Nyquist plots of cells measured (a) in the dark and (b) under illumination.

DOI: 10.1021/acs.inorgchem.5b00661
Inorg. Chem. 2015, 54, 7742−7752

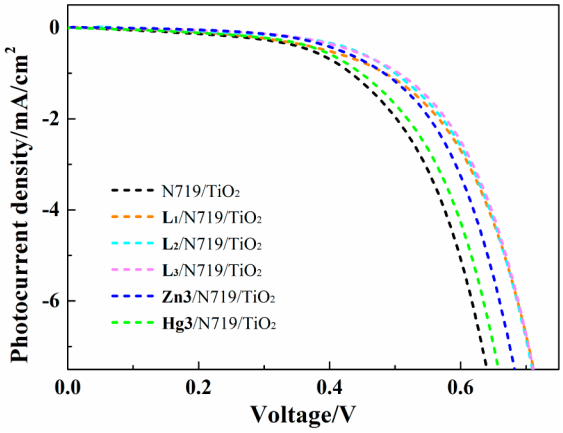

Figure 10. *J*−*V* curves of cells measured in the dark.

declined dark current, the electron back reaction with I_3^- was successfully suppressed in the electrolyte by forming a compact layer with N719 through cosensitizing the ligands $\mathbf{L_1}$−$\mathbf{L_3}$ and complexes **Zn3**/**Hg3**. It is a vital element to reduce the current leakage in DSSC and enhance its efficiency. At the same time, the declined dark current caused an increase of V_{oc}, which supports the results of EIS under dark conditions.

CONCLUSION

In summary, six transition metal Zn(II)/Hg(II) complexes with (*E*)-*N*-(6-methoxypyridin-2-yl)(CH═NAr) (Ar = C_6H_5, $\mathbf{L_1}$; 2-MeC_6H_4, $\mathbf{L_2}$; 2,4,6-$Me_3C_6H_2$, $\mathbf{L_3}$) ligands were synthesized. Crystal structure analysis reveals that these mononuclear complexes can aggregate into different dimensional supramolecular structures (1D for **Hg3**; 2D for **Zn2**, **Hg2**; 3D for **Zn1**, **Hg1**, and **Zn3**) through noncovalent bond interactions. Upon irradiation with UV light, the emission of complexes **Zn1**−**Zn3** and **Hg1**−**Hg3** could be finely tuned from green (480−540 nm) in the solid state to blue (402−425 nm) in acetonitrile solution. In addition, the emission intensities and maximum wavelengths could be fine tuned by varying the center metals or substituents on the ligands. DSSCs that employ $\mathbf{L_1}$−$\mathbf{L_3}$ and complexes **Zn3**/**Hg3** as cosensitizers show that the performance of N719-sensitized solar cells is significantly enhanced. Among these cosensitized DSSCs, the $\mathbf{L_3}$/N719 device demonstrated the best overall conversion efficiency of 7.25% with a higher J_{sc} of 18.18 mA/cm^2, much higher by ca. 41% than that of an individual N719-sensitized device (5.14%). These results provide beneficial information for designing and synthesizing cosensitizers as well as improving the efficiency of DSSCs. Nevertheless, further investigation toward this aspect is underway.

EXPERIMENTAL SECTION

Chemicals and Solvents. All starting materials such as anilne derivants (aniline, 2-methylaniline, and 2,4,6-trimethylaniline), 6-methoxy-2-pyridinecarboxaldehyde, and metal salts ($ZnCl_2$/$HgCl_2$) were obtained from commercial sources. The solvents like methanol, acetonitrile, and dichloromethane were reagent grade and dried before using.

Instrumentation. Elemental analyses were carried out on a Perkin-Elmer 2400 automatic analyzer. FT-IR spectral data (4000−400 cm^{-1}) were collected by a Nicolet impact 410 FT-IR spectrometer. ^{1}H NMR spectra were obtained using a Bruker Avance-400 MHz spectrometer with Si(CH_3)$_4$ as internal standard. A THERMO Finnigan LCQ Advantage Max ion trap mass spectrometer was used to collect ESI-MS spectra. A Perkin-Elmer Lambda 35 spectrometer was used to measure the UV−vis absorption spectra of ligands and complexes. The emission luminescence and lifetime properties were recorded with an Edinburgh FLS 920 fluorescence spectrometer. Cyclic voltammetry was performed on a CHI660d electrochemical workstation (Shanghai, China). All samples were dissolved in 10 mL of EtOH containing 0.1 M teterabutylammonium hexafluorophosphate ($TBAPF_6$) as the supporting electrolyte.

Synthesis. *General Procedure for (E)-N-(6-Methoxypyridin-2-ylmethylene)arylamine Ligands* ($\mathbf{L_1}$−$\mathbf{L_3}$). Ligands $\mathbf{L_1}$−$\mathbf{L_3}$ were prepared by analogous methods. A 16.63 mmol amount of 6-methoxy-2-pyridinecarboxaldehyde (2.0 mL) was added into 1 equiv of aniline derivatives (aniline (1.53 mL), 2-methylaniline (1.78 mL), or 2,4,6-trimethylaniline (2.34 mL)) in anhydrous methanol (20 mL). The resultant solutions were set at reflux for ca. 8−12 h and subsequently concentrated under reduced pressure to obtain yellow crude products. $\mathbf{L_1}$ and $\mathbf{L_2}$ were yellow oil liquids. After recrystallization from methanol, yellow block crystals of ligand $\mathbf{L_3}$ were obtained.

N-((6-Methoxypyridin-2-yl)methylene)aniline ($\mathbf{L_1}$). Yield: 3.25 g (92%). Anal. Calcd for $\mathbf{L_1}$ [$C_{13}H_{12}N_2O$ (212.25)]: C, 73.56; H, 5.70; N, 13.20. Found: C, 73.35; H, 5.61; N, 13.55. ^{1}H NMR ($CDCl_3$, 400 MHz, ppm): 8.48 (s, 1H, *H*C═N), 7.78 (d, 1H, pyridine-H_5), 7.68 (t, 1H, pyridine-H_4), 7.42 (d, 1H, pyridine-H_3), 6.82−7.39 (m, 5H, phene-*H*), 4.00 (s, 3H, −O*C*H_3). FT-IR (KBr, cm^{-1}): 3386, 3060, 2948, 1629 (s, $\nu_{C=N}$), 1589, 1486, 1467, 1430, 1413, 1334, 1267, 1205, 1145, 1074, 1031, 987, 908, 860, 804, 755, 730, 694, 647, 605, 545, 528, 458. ESI-MS: m/z = 213.1 [M + H]$^+$.

(E)-2-Methyl-N-((6-methoxypyridin-2-yl)methylene)aniline ($\mathbf{L_2}$). Yield: 3.34 g (89%). Anal. Calcd for $\mathbf{L_2}$ [$C_{14}H_{14}N_2O$ (226.28)]: C, 74.31; H, 6.24; N, 12.38. Found: C, 74.45; H, 6.35; N, 12.23. ^{1}H NMR ($CDCl_3$, 400 MHz, ppm): 8.37 (s, 1H, *H*C═N), 7.84 (d, 1H, pyridine-H_5), 7.68 (t, 1H, pyridine-H_4), 7.24 (d, 1H, pyridine-H_3), 6.81−7.22 (m, 4H, phene-*H*), 4.00 (s, 3H, −O*C*H_3), 2.38 (s, 3H, −*C*H_3). FT-IR (KBr, cm^{-1}): 3064, 2948, 2856, 1633 (s, $\nu_{C=N}$), 1591, 1575, 1484, 1467, 1430, 1322, 1265, 1214, 1187, 1145, 1112, 1074, 1033, 987, 867, 804, 757, 730, 644, 576, 532, 457. ESI−MS: m/z = 227.2 [M + H]$^+$.

(E)-2,4,6-Trimethyl-N-((6-methoxypyridin-2-yl)methylene)aniline ($\mathbf{L_3}$). Yield: 2.95 g (70%). Anal. Calcd for $\mathbf{L_3}$ [$C_{16}H_{18}N_2O$ (254.32)]: C, 75.56; H, 7.13; N, 11.01. Found: C, 75.68; H, 7.05; N, 11.22. ^{1}H NMR ($CDCl_3$, 400 MHz, ppm): 8.20 (s, 1H, *H*C═N), 7.86 (d, 1H, pyridine-H_5), 7.70 (t, 1H, pyridine-H_4), 6.89 (s, 2H, phene-*H*), 6.85 (d, 1H, pyridine-H_3), 3.98 (s, 3H, −O*C*H_3), 2.13−2.29 (m, 9H, −*C*H_3). FT-IR (KBr, cm^{-1}): 3432, 3080, 2948, 2857, 1646 (s, $\nu_{C=N}$), 1589, 1572, 1466, 1442, 1423, 1384, 1375, 1333, 1321, 1267, 1231, 1205, 1144, 1076, 1034, 986, 974, 860, 839, 816, 807, 733, 651, 629, 576, 505, 494, 465. ESI-MS: m/z = 255.3 [M + H]$^+$.

General Procedure for Six Zn(II)/Hg(II) Complexes. The complexes were synthesized by dissolving metal salts $ZnCl_2$ (27.3 mg) or $HgCl_2$ (54.3 mg) and 1 mol equiv of the respective Schiff-base ligands in anhydrous solutions (methanol or acetonitrile or methanol/dichloromethane). The yellow solutions were refluxed for 12 h and subsequently filtered. X-ray quality single crystals of six Zn(II)/Hg(II) complexes were grown from slow evaporation of their solutions (Scheme 1).

ZnL_1Cl_2 (**Zn1**). Yield: 45.3 mg (65%). Anal. Calcd for **Zn1** [$C_{13}H_{12}Cl_2N_2OZn$ (348.54)]: C, 44.80; H, 3.47; N, 8.04. Found: C, 44.94; H, 3.35; N, 7.98. ^{1}H NMR ($CDCl_3$, 400 MHz, ppm): 8.64 (s, 1H, *H*C═N), 8.14 (t, 1H, pyridine-H_5), 7.80 (d, 1H, pyridine-H_4), 7.78 (d, 1H, pyridine-H_3), 7.24−7.54 (m, 5H, phene-*H*), 4.27 (s, 3H, −O*C*H_3). FT-IR (KBr, cm^{-1}): 3435, 3081, 2981, 2874, 1620 (w, $\nu_{C=N}$), 1595, 1569, 1478, 1428, 1374, 1298, 1237, 1173, 1099, 1016, 961, 910, 869, 803, 769, 737, 684, 665, 641, 599, 549, 518, 478. ESI-MS: m/z = 313.1 [M − Cl]$^+$.

HgL_1Cl_2 (**Hg1**). Yield: 59.0 mg (61%). Anal. Calcd for **Hg1** [$C_{13}H_{12}Cl_2N_2OHg$ (483.74)]: C, 32.28; H, 2.50; N, 5.79. Found: C, 32.07; H, 2.66; N, 5.83. ^{1}H NMR ($CDCl_3$, 400 MHz, ppm): 8.59 (s, 1H, *H*C═N), 7.85 (t, 1H, pyridine-H_5), 7.65 (d, 1H, pyridine-H_4), 7.44 (d, 1H, pyridine-H_3), 6.96−7.43 (m, 5H, phene-*H*), 4.07 (s, 3H,

DOI: 10.1021/acs.inorgchem.5b00661
Inorg. Chem. 2015, 54, 7742−7752

$-OCH_3$). FT-IR (KBr, cm^{-1}): 3435, 3062, 2955, 2869, 1628 (w, $\nu_{C=N}$), 1586, 1570, 1474, 1425, 1373, 1299, 1237, 1176, 1096, 1004, 954, 861, 817, 772, 742, 685, 590, 546, 517, 469. ESI-MS: m/z = 449.1 $[M - Cl]^+$.

*ZnL_2Cl_2 (**Zn2**).* Yield: 42.1 mg (58%). Anal. Calcd for **Zn2** [$C_{14}H_{14}Cl_2N_2OZn$ (362.56)]: C, 46.38; H, 3.89; N, 7.73. Found: C, 46.54; H, 3.97; N, 7.50. ^1H NMR ($CDCl_3$, 400 MHz, ppm): 8.37 (s, 1H, *HC*=N), 8.16 (t, 1H, pyridine-H_5), 7.80 (d, 1H, pyridine-H_4), 7.53 (d, 1H, pyridine-H_3), 6.97−7.27 (m, 4H, phene-*H*), 4.27 (s, 3H, $-OCH_3$), 2.48 (s, 3H, $-CH_3$). FT-IR (KBr, cm^{-1}): 3434, 3079, 2985, 2857, 1630 (m, $\nu_{C=N}$), 1600, 1580, 1481, 1428, 1372, 1303, 1234, 1211, 1187, 1175, 1116, 1099, 1088, 1040, 1016, 993, 964, 877, 866, 811, 795, 770, 740, 719, 664, 604, 579, 541, 507, 480, 456. ESI-MS: m/z = 227.2 $[M - Zn-2Cl]^+$.

*HgL_2Cl_2 (**Hg2**).* Yield: 53.8 mg (54%). Anal. Calcd for **Hg2** [$C_{14}H_{14}Cl_2N_2OHg$ (497.76)]: C, 33.78; H, 2.84; N, 5.63. Found: C, 33.96; H, 2.57; N, 5.51. ^1H NMR ($CDCl_3$, 400 MHz, ppm): 8.48 (s, 1H, *HC*=N), 7.97 (t, 1H, pyridine-H_5), 7.73 (t, 1H, pyridine-H_4), 7.58 (d, 1H, pyridine-H_3), 6.97−7.10 (m, 4H, phene-*H*), 4.03 (s, 3H, $-OCH_3$), 2.43 (s, 3H, $-CH_3$). FT-IR (KBr, cm^{-1}): 3435, 3075, 2943, 2834, 1619 (m, $\nu_{C=N}$), 1582, 1571, 1477, 1460, 1424, 1375, 1312, 1297, 1234, 1186, 1177, 1115, 1097, 1034, 1011, 992, 960, 948, 871, 860, 795, 768, 745, 730, 718, 658, 638, 600, 572, 536, 515, 473, 458, 446. ESI-MS: m/z = 499.7 $[M + H]^+$, 463.2 $[M - Cl]^+$.

*ZnL_3Cl_2 (**Zn3**).* Yield: 57.0 mg (73%). Anal. Calcd for **Zn3** [$C_{16}H_{18}Cl_2N_2OZn$ (390.61)]: C, 49.20; H, 4.65; N, 7.17. Found: C, 49.57; H, 4.53; N, 7.38. ^1H NMR ($CDCl_3$, 400 MHz, ppm): 8.27 (s, 1H, *HC*=N), 8.15 (d, 1H, pyridine-H_5), 7.49 (d, 1H, pyridine-H_4), 7.32 (d, 1H, pyridine-H_3), 6.93 (s, 2H, phene-*H*), 4.29 (s, 3H, $-OCH_3$), 2.29 (m, 9H, $-CH_3$). FT-IR (KBr, cm^{-1}): 3435, 3085, 2944, 2919, 2862, 1637 (m, $\nu_{C=N}$), 1598, 1575, 1482, 1431, 1368, 1308, 1296, 1226, 1201, 1178, 1145, 1093, 1039, 1014, 977, 950, 895, 856, 806, 749, 740, 641, 595, 583, 500, 449. ESI-MS: m/z = 355.2 $[M - Cl]^+$, 318.3 $[M - 2Cl]^+$.

*HgL_3Cl_2 (**Hg3**).* Yield: 69.4 mg (66%). Anal. Calcd for **Hg3** [$C_{16}H_{18}Cl_2N_2OHg$ (525.81)]: C, 36.55; H, 3.45; N, 5.33. Found: C, 36.88; H, 3.38; N, 5.20. ^1H NMR ($CDCl_3$, 400 MHz): 8.44 (s, 1H, *HC*=N), 8.02 (t, 1H, pyridine-H_5), 7.42 (d, 1H, pyridine-H_4), 7.18 (d, 1H, pyridine-H_3), 6.92 (s, 2H, phene-*H*), 4.16 (s, 3H, $-OCH_3$), 2.24−2.30 (m, 9H, $-CH_3$) ppm. FT-IR (KBr, cm^{-1}): 3434, 3085, 2968, 2915, 2861, 1637 (m, $\nu_{C=N}$), 1590, 1575, 1474, 1431, 1379, 1367, 1293, 1228, 1199, 1177, 1147, 1085, 1037, 1006, 977, 949, 898, 860, 836, 806, 749, 735, 640, 594, 566, 496, 435. ESI-MS: m/z = 475.2 $[M - Cl - CH_3]^+$.

Crystallographic Data Collection and Structure Refinements. Suitable crystals of ligand $\mathbf{L_3}$ and six complexes **Zn1**−**Zn3** and **Hg1**−**Hg3** were selected and mounted on a Rigaku R-AXIS RAPID IP diffractometer. Diffraction data were collected using graphite-monochromatized Mo Kα radiation (λ = 0.71073 Å). The structures were solved with direct methods[44] and refined with full-matrix least-squares on F^2. All hydrogen atoms were constrained in geometric positions to their parent atoms, and non-hydrogen atoms were refined anisotropically. The detailed crystal structure refinement data of $\mathbf{L_3}$, **Zn1**−**Zn3**, and **Hg1**−**Hg3** are summarized in Table 1. The CCDC numbers are 1046956, 1046957, 1046958, 1046959, 1046960, 1046961, and 1046962 for **Zn1**, **Hg1**, **Zn2**, **Hg2**, $\mathbf{L_3}$, **Zn3**, and **Hg3**, respectively.

Dye-Sensitized Solar Cell Fabrication. TiO_2 paste was prepared according to the following procedure. A fluorine-doped tin oxide (FTO, 15 Ω sq^{-1}) conductive glass (NSG) was screen printed with a titania film, which was dried at 100 °C for 5 min, and this was done six times. TiO_2 film was then sintered at 500 °C for 15 min. After cooling to 80 °C, the photoanodes were stained by immersing them into ligand ($\mathbf{L_1}$−$\mathbf{L_3}$) or complex (**Zn3** and **Hg3**) in absolute ethanol solution (0.3 mM) for 2 h; after this, it was washed with ethanol. Finally, it was further immersed into N719 in absolute ethanol solution (0.3 mM) for 14 h, followed by washing with ethanol. The electrolyte used contained 0.5 M LiI, 0.05 M I_2, and 0.1 M *tert*-butylpyridine in a 1:1 solvent mixture of acetonitrile/propylene carbonate.

Device Characterization. The current−voltage (J−V) characteristics of the DSSCs were measured using a Keithley source meter (model 2400) in the dark and under illumination. The incident light intensity was 100 mW cm^{-2}, calibrated by a standard silicon solar cell. During the I−V measurement, a 0.16 cm^2 mask was used to get a uniform working area for all cells. The incident photon-to-current conversion efficiency (IPCE) spectra of the DSSCs were measured using an EQE/IPCE spectral response system (Newport). The electrochemical impedance spectra, in the dark and under illumination, were recorded using a CHI660D electrochemical workstation (Chenhua, China); measurements were taken under standard global AM1.5 solar irradiation over a frequency ranging from 0.1 to 10^5 Hz.

■ ASSOCIATED CONTENT

Supporting Information

X-ray crystallographic files (CIF), structural information for **Zn1**−**Zn3** and **Hg1**−**Hg3**, FT-IR spectra, ^1H NMR spectra, PXRD patterns, luminescent data, and selected bond lengths and angles for **Zn1**−**Zn3** and **Hg1**−**Hg3**. The Supporting Information is available free of charge on the ACS Publications website at DOI: 10.1021/acs.inorgchem.5b00661.

■ AUTHOR INFORMATION

Corresponding Authors

*E-mail: fanruiqing@hit.edu.cn.

*E-mail: ylyang@hit.edu.cn.

Notes

The authors declare no competing financial interest.

■ ACKNOWLEDGMENTS

This work was supported by the National Natural Science Foundation of China (Grants 21371040 and 21171044), the National key Basic Research Program of China (973 Program, No. 2013CB632900), Fundamental Research Funds for the Central Universities (Grant No. HIT.IBRSEM.A.201409), and the Program for Innovation Research of Science in Harbin Institute of Technology (PIRS of HIT No. A201416 and B201414).

■ REFERENCES

(1) Kuda-Wedagedara, A. N. W.; Wang, C. C.; Martin, P. D.; Allen, M. J. *J. Am. Chem. Soc.* **2015**, *137*, 4960.

(2) Jiang, K.; Sun, S.; Zhang, L.; Lu, Y.; Wu, A.; Cai, C. Z.; Lin, H. W. *Angew. Chem., Int. Ed.* **2015**, *54*, 5360.

(3) Raja, D. S.; Lin, P. C.; Liu, W. R.; Zhan, J. X.; Fu, X. Y.; Lin, C. H. *Inorg. Chem.* **2015**, *54*, 4268.

(4) (a) O'Regan, B.; Grätzel, M. *Nature* **1991**, *353*, 737. (b) Cabau, L.; Kumar, C. V.; Moncho, A.; Clifford, J. N.; López, N.; Palomares, E. *Energy Environ. Sci.* **2015**, *8*, 1368. (c) Bisquert, J.; Cahen, D.; Hodes, G.; Rühle, S.; Zaban, A. *J. Phys. Chem. B* **2004**, *108*, 8106.

(5) (a) Zhao, H. C.; Harney, J. P.; Huang, Y. T.; Yum, J. H.; Nazeeruddin, M. K.; Grätzel, M.; Tsai, M. K.; Rochford, J. *Inorg. Chem.* **2012**, *51*, 1. (b) O'Donnell, R. M.; Johansson, P. G.; Abrahamsson, M.; Meyer, G. J. *Inorg. Chem.* **2013**, *52*, 6839. (c) Li, G.; Yella, A.; Brown, D. G.; Gorelsky, S. I.; Nazeeruddin, M. K.; Grätzel, M.; Berlinguette, C. P.; Shatruk, M. *Inorg. Chem.* **2014**, *53*, 5417.

(6) Kwok, E. C. H.; Chan, M. Y.; Wong, K. M. C.; Yam, V. W. W. *Chem.—Eur. J.* **2014**, *20*, 3142.

(7) (a) Mei, J. G.; Bao, Z. N. *Chem. Mater.* **2014**, *26*, 604. (b) Shavaleev, N. M.; Xie, G. H.; Varghese, S.; Cordes, D. B.; Slawin, A. M. Z.; Momblona, C.; Ortí, E.; Bolink, H. J.; Samuel, I. D. W.; Zysman-Colman, E. *Inorg. Chem.* **2015**, *54*, 5907.

(8) Yang, Q. Y.; Pan, M.; Wei, S. C.; Li, K.; Du, B. B.; Su, C. Y. *Inorg. Chem.* **2015**, *54*, 5707.

(9) (a) Tong, W. L.; Yiu, S. M.; Chan, M. C. W. *Inorg. Chem.* **2013**, *52*, 7114. (b) Servati-Gargari, M.; Mahmoudi, G.; Batten, S. R.;

DOI: 10.1021/acs.inorgchem.5b00661
Inorg. Chem. 2015, 54, 7742−7752

Stilinović, V.; Butler, D.; Beauvais, L.; Kassel, W. S.; Dougherty, W. G.; VanDerveer, D. *Cryst. Growth Des.* **2015**, *15*, 1336.
(10) Wang, X. M.; Wang, P.; Fan, R. Q.; Xu, M. Y.; Qiang, L. S.; Wei, L. G.; Yang, Y. L.; Wang, Y. L. *Dalton Trans.* **2015**, *44*, 5179.
(11) Stergiopoulos, T.; Falaras, P. *Adv. Energy Mater.* **2012**, *2*, 616.
(12) (a) Namba, K.; Osawa, A.; Nakayama, A.; Mera, A.; Tano, F.; Chuman, Y.; Sakuda, E.; Taketsugu, T.; Sakaguchi, K.; Kitamurac, N.; Tanino, K. *Chem. Sci.* **2015**, *6*, 1083. (b) Wei, L. G.; Yang, Y. L.; Fan, R. Q.; Wang, P.; Dong, Y. W.; Zhou, W.; Luan, T. Z. *J. Power Sources* **2015**, *293*, 203.
(13) Gao, S.; Fan, R. Q.; Wang, X. M.; Qiang, L. S.; Wei, L. G.; Wang, P.; Zhang, H. J.; Yang, Y. L.; Wang, Y. L. *J. Mater. Chem. A* **2015**, *3*, 6053.
(14) Gao, S.; Fan, R. Q.; Wang, X. M.; Qiang, L. S.; Wei, L. G.; Wang, P.; Yang, Y. L.; Wang, Y. L.; Luan, T. Z. *RSC Adv.* **2015**, *5*, 43705.
(15) (a) Baran, P.; Boca, R.; Breza, M.; Elias, H.; Fuess, H.; Jorik, V.; Klement, R.; Svoboda, I. *Polyhedron* **2002**, *21*, 1561. (b) Gong, X.; Ge, Y. Y.; Fang, M.; Gu, Z. G.; Zheng, S. R.; Li, W. S.; Hu, S. J.; Li, S. B.; Cai, Y. P. *CrystEngComm* **2011**, *13*, 6911.
(16) Kumar, J.; Sarma, M. J.; Phukan, P.; Das, D. K. *Dalton Trans.* **2015**, *44*, 4576.
(17) Zhang, L. Y.; Sun, L. Y.; Li, X. Y.; Tian, Y. L.; Yuan, G. Z. *Dalton Trans.* **2015**, *44*, 401.
(18) Franks, M.; Gadzhieva, A.; Ghandhi, L.; Murrell, D.; Blake, A. J.; Davies, E. S.; Lewis, W.; Moro, F.; McMaster, J.; Schröder, M. *Inorg. Chem.* **2013**, *52*, 660.
(19) Bondi, A. *J. Phys. Chem.* **1964**, *68*, 441.
(20) (a) Hong, X. J.; Wang, M. F.; Jia, H. Y.; Li, W. X.; Li, J.; Liu, Y. T.; Jin, H. G.; Cai, Y. P. *New J. Chem.* **2013**, *37*, 933. (b) Wang, M. F.; Hong, X. J.; Zhan, Q. G.; Jin, H. G.; Liu, Y. T.; Zheng, Z. P.; Xu, S. H.; Cai, Y. P. *Dalton Trans.* **2012**, *41*, 11898.
(21) Baul, T. S. B.; Kundu, S.; Mitra, S.; Höpfl, H.; Tiekink, E. R. T.; Linden, A. *Dalton Trans.* **2013**, *42*, 1905.
(22) Maxim, C.; Tuna, F.; Madalan, A. M.; Avarvari, N.; Andruh, M. *Cryst. Growth Des.* **2012**, *12*, 1654.
(23) (a) Fan, R. Q.; Wang, L. Y.; Chen, H.; Zhou, G. P.; Yang, Y. L.; Hasi, W. L. J.; Cao, W. W. *Polyhedron* **2012**, *33*, 90. (b) Yang, X. L.; Xie, M. H.; Zou, C.; Wu, C. D. *CrystEngComm* **2011**, *13*, 6422.
(24) (a) Shen, J. J.; Li, M. X.; Wang, Z. X.; Duan, C. Y.; Zhu, S. R.; He, X. *Cryst. Growth Des.* **2014**, *14*, 2818. (b) Allendorf, M. D.; Bauer, C. A.; Bhakta, R. K.; Houk, R. J. T. *Chem. Soc. Rev.* **2009**, *38*, 1330. (c) Majumder, S.; Mandal, L.; Mohanta, S. *Inorg. Chem.* **2012**, *51*, 8739.
(25) (a) Chen, J. Q.; Cai, Y. P.; Fang, H. C.; Zhou, Z. Y.; Zhan, X. L.; Zhao, G.; Zhang, Z. *Cryst. Growth Des.* **2009**, *9*, 1605. (b) Liu, Z. F.; Wu, M. F.; Zheng, F. K.; Wang, S. H.; Zhang, M. J.; Chen, J.; Xiao, Y.; Guo, G. C.; Wu, A. Q. *CrystEngComm* **2013**, *15*, 7038.
(26) Stylianou, K. C.; Heck, R.; Chong, S. Y.; Bacsa, J.; Jones, J. T. A.; Khimyak, Y. Z.; Bradshaw, D.; Rosseinsky, M. J. *J. Am. Chem. Soc.* **2010**, *132*, 4119.
(27) (a) Fan, R. Q.; Zhang, Y. J.; Yin, Y. B.; Su, Q.; Yang, Y. L.; Hasi, W. L. J. *Synth. Met.* **2009**, *159*, 1106. (b) Wang, L. Y.; Fan, R. Q.; Wang, P.; Yang, Y. L. *Inorg. Chem. Commun.* **2012**, *23*, 54.
(28) (a) Seward, C.; Chan, J.; Song, D.; Wang, S. N. *Inorg. Chem.* **2003**, *42*, 1112. (b) Antina, E. V.; Kuznetsova, R. T.; Antina, L. A.; Guseva, G. B.; Dudina, N. A.; V'yugin, A. I.; Solomonov, A. V. *Dyes Pigm.* **2015**, *113*, 664.
(29) (a) Wei, T. B.; Gao, G. Y.; Qu, W. J.; Shi, B. B.; Lin, Q.; Yao, H.; Zhang, Y. M. *Sens. Actuators, B* **2014**, *199*, 142. (b) Li, L. Q.; Yuan, L.; Liu, Z. H. *J. Fluoresc.* **2014**, *24*, 1357.
(30) Mandal, H.; Chakrabartty, S.; Ray, D. *RSC Adv.* **2014**, *4*, 65044.
(31) Murugan, K. D.; Natarajan, P. *Eur. Polym. J.* **2011**, *47*, 1664.
(32) Kundu, N.; Audhya, A.; Abtab, S. M. T.; Ghosh, S.; Tiekink, E. R. T.; Chaudhury, M. *Cryst. Growth Des.* **2010**, *10*, 1269.
(33) Wang, M. K.; Chamberland, N.; Breau, L.; Moser, J. E.; Humphry-Baker, R.; Marsan, B.; Zakeeruddin, S. M.; Grätzel, M. *Nat. Chem.* **2010**, *2*, 385.
(34) Sharma, G. D.; Singh, S. P.; Kurchania, R.; Ball, R. J. *RSC Adv.* **2013**, *3*, 6036.
(35) Boschloo, G.; Halggman, L.; Hagfeldt, A. *J. Phys. Chem. B* **2006**, *110*, 13144.
(36) Li, W. H.; Liu, Z. H.; Wu, H. Z.; Cheng, Y. B.; Zhao, Z. X.; He, H. S. *J. Phys. Chem. C* **2015**, *119*, 5265.
(37) Cardona, C. M.; Li, W.; Kaifer, A. E.; Stockdale, D.; Bazan, G. C. *Adv. Mater.* **2011**, *23*, 2367.
(38) Wu, W. J.; Zhang, J.; Yang, H. B.; Jin, B.; Hu, Y.; Hua, J. L.; Jing, C.; Long, Y. T.; Tian, H. *J. Mater. Chem.* **2012**, *22*, 5382.
(39) Zhang, H.; Fan, J.; Iqbal, Z.; Kuang, D. B.; Wang, L. Y.; Cao, D. R.; Meier, H. *Dyes Pigm.* **2013**, *99*, 74.
(40) (a) Hagfeldt, A.; Boschloo, G.; Sun, L.; Kloo, L.; Pettersson, H. *Chem. Rev.* **2010**, *110*, 6595. (b) Saxena, V.; Veerender, P.; Gusain, A.; Jha, P.; Singh, J.; Koiry, S. P.; Varde, P. V.; Chauhan, A. K.; Aswal, D. K.; Gupta, S. K. *Org. Electron.* **2013**, *14*, 3098.
(41) Malara, F.; Cannavale, A.; Carallo, S.; Gigli, G. *ACS Appl. Mater. Interfaces* **2014**, *6*, 9290.
(42) (a) Longo, C.; Nogueira, A. F.; Paoli, M. D.; Cachet, H. *J. Phys. Chem. B* **2002**, *106*, 5925. (b) Thomas, K. R. J.; Hsu, Y. C.; Lin, J. T.; Lee, K. M.; Ho, K. C.; Lai, C. H.; Cheng, Y. M.; Chou, P. T. *Chem. Mater.* **2008**, *20*, 1830. (c) Shen, P.; Tang, Y. H.; Jiang, S. H.; Chen, H. J.; Zheng, X. Y.; Wang, X. Y.; Zhao, B.; Tan, S. T. *Org. Electron.* **2011**, *12*, 125.
(43) Ito, S.; Liska, P.; Comte, P.; Charvet, R.; Pechy, P.; Bach, U.; Schmidt-Mende, L.; Zakeeruddin, S. M.; Kay, A.; Nazeeruddin, M. K.; Grätzel, M. *Chem. Commun.* **2005**, *34*, 4351.
(44) Sheldrick, G. M. *SHELXTL NT Crystal Structure Analysis Package*, Version 5.10; Bruker AXS, Analytical X-ray System: Madison, WI, 1999.

DOI: 10.1021/acs.inorgchem.5b00661
Inorg. Chem. 2015, 54, 7742−7752